JOURNAL OF AIRCRAFT
Vol. 48, No. 3, May–June 2011

Ultrasonic De-Icing of Wind-Tunnel Impact Icing

Jose Palacios,* Edward Smith,† and Joseph Rose‡
Pennsylvania State University, University Park, Pennsylvania 16802
and
Roger Royer§
FBS Worldwide, Inc., State College, Pennsylvania 16803

DOI: 10.2514/1.C031201

Ultrasonic excitation has proven to provide ice-interface transverse shear stresses exceeding the adhesion strength of freezer ice to various metals, promoting instantaneous ice delamination. Wind-tunnel impact ice presents challenges that are not encountered when removing freezer ice. The low-power, nonthermal ultrasonic de-icing concept is investigated under impact-icing conditions in an icing wind tunnel. In this research effort, ultrasonic actuator disks excite isotropic plates and airfoil-shaped structures that are representative of helicopter leading-edge protection-cap shapes. Off-the-shelf ultrasonic actuators are used to create ice-interface shear stresses sufficient to promote instantaneous ice delamination of thin layers of impact ice (less than 3 mm thick). A steel plate of 30.48 cm × 30.48 cm × 1 mm was actuated by three lead zirconate titanate disks excited at their ultrasonic radial mode. The ultrasonic vibration introduced transverse shear stresses that prevented ice formation on top of the actuator locations for a fraction of the power required with electrothermal systems used in helicopter rotor blades (0.18 W/cm² vs 3.8 W/cm²). Experiments also showed ice delamination in areas of the plates where transverse shear stresses were concentrated. As ice thicknesses reached a critical value of approximately 1.2 mm, ice debonded from those steel-plate areas. A model of the three disk actuated steel plate was created and correlated with experimental results observed during impact-icing test experiments. Both, the predicted ultrasonic modes of the system and the ice-shedding areas agreed with experimental results. In addition, a second set of experiments involving NACA 0012 airfoil-shaped structures were conducted. Actuators located on the top and bottom surfaces of the leading-edge cap were actuated with an input power as low as 200 W (32 kHz ultrasonic mode). Thin layers of ice (less than 2 mm thick) constantly delaminated from the leading edge of the airfoil on those regions where stress concentrations were predicted.

Nomenclature

c^E	=	elastic stiffness at constant electric field, N/m^2
D	=	electric displacement vector, C/m^2
E	=	applied external electric field vector, V/m
e	=	piezoelectric coupling, N/(mV)
F	=	applied mechanical force, N
I	=	current, A
K_{uu}	=	elastic stiffness matrix, N/m
$K_{u\varphi}$	=	piezoelectric stiffness matrix, N/V
$K_{\varphi\varphi}$	=	dielectric matrix, F
Q	=	vector of the nodal charges, C
S	=	strain vector, dimensionless
T	=	stress vector, N/m^2
U	=	elastic displacement, m
Z	=	impedance, Ω
ε^S	=	dielectric stiffness at constant strain, F/m
σ_{XY}	=	shear stress, N/m^2
σ_{ZX}	=	transverse shear stress, N/m^2
φ	=	electric potential, V
ω	=	frequency, rad/s

Received 30 July 2010; revision received 18 November 2010; accepted for publication 25 November 2010.

*Research Associate, Department of Aerospace Engineering, 229 Hammond Building. Member AIAA.
†Professor Aerospace Engineering, 231D Hammond Building. Member AIAA.
‡Paul Morrow Professor, Department of Engineering Science and Mechanics, 0212 Earth and Engineering Sciences.
§Director of Technology and Business Development, 143 Hawbaker Industrial Drive, Suite 102.

I. Introduction

HELICOPTER rotors are more susceptible to icing than the rest of the fuselage or fixed wing vehicles. Rotors impact more supercooled water particles per second than the rest of the fuselage. In addition, the higher collection efficiency of rotor airfoils makes them accrete ice at a higher rate than thicker airfoils. While fixed wing aircraft cruise at altitudes above icing conditions, rotorcraft vehicles operate in atmospheric conditions where supercooled water particles are found. Ice accretion can be critically dangerous, as it can modify the vehicles aerodynamics, create excessive vibration, increase weight and drag [1], and introduce ballistic concerns as ice sheds off. The only standard de-icing systems qualified by the Federal Aviation Administration is based on electrothermal energy, used to melt the ice interface between accreted ice and the leading-edge erosion-protection cap of the rotor. Extensive ice testing of the S-92 conducted by Flemming et al. [2–4], has demonstrated the reliability of thermal de-icing systems for larger vehicles. For these types of vehicles (greater than 10,000 lb empty weight), ice accretion is not a major concern due to the availability of sufficient electrical power and payload to implement robust electrothermal ice protection systems. The thermal de-icing mechanism is run cyclically in order to limit power consumption or introduce excessive heating of the leading-edge structure (which could cause composite delamination). Such a system requires large amounts of energy (3.9 W/cm^2 or 25 W/in.^{2}) and contributes to an undesired increase in the overall weight of the system and cost of the blade. The high power consumption of this system limits the time that it can be active and the surface area that can be protected. Those areas not protected during de-icing continue to accumulate ice until the heating mats under that specific leading-edge region are turned on. During some occasions, melted ice might flow to the aft portion of the blade (where there are

no heating mats) to refreeze. Since the electrothermal de-icing system sublimates the ice interface, ice shedding occurs under centrifugal loading. Released ice patches that could reach up to 7.6 mm in thickness [5] are a ballistic concern for some vehicles. The system relies on the thermal conductivity of isotropic materials to protect the leading edge of the blade from erosion. For this reason, electrothermal de-icing is not suitable for new polymer-based leading-edge protection materials that present lower thermal conductivity. A major disadvantage of electrothermal de-icing is that the electrical power required substantially exceeds the normal helicopter electrical system capacity, necessitating a secondary electrical system with redundant, dual alternator features [5]. The weight related to the required electrical power can be as large as 112 kg (245 lb) on a 4300 kg (9500 lb) gross weight helicopter [5].

Because of mentioned drawbacks, particularly power generation weight and system cost constraints, medium- and small-sized vehicles avoid the installation of electrothermal de-icing systems, also limiting operation in icing environments. The need for a low-power, nonthermal, reliable de-icing system is critical to the operation of small and medium size helicopters in all weather conditions. Such a system would also increase icing time operation capabilities of larger vehicles. In addition, a nonthermal de-icing system would allow for the implementation of erosion resistant, low thermal conductivity coatings at the leading edge of the blade.

A passive ice-phobic coating would be the ideal solution to helicopter rotor blade ice accretion. Ice-phobic coatings quickly degrade under erosion conditions inherent to rotor blade operations (rain, sand particles impact), losing their ice-phobic properties. An erosion resistant and ice-phobic material has not been found to date.

The search for reliable low-power, nonthermal de-icing system has generated several impulsive de-icing systems aiming to crack and shed off accreted ice. Electroimpulsive [5], electromagnetic impulsive—eddy current repulsion [6], pneumatic inflation [7], shape memory alloy stresses, and structural resonance [8,9] are some of the de-icing methods that have been studied. All of these methods remain conceptual and present drawbacks. For example pneumatic de-icing systems rely on inflatable boots at the leading edge that tend to erode during operation. Electroimpulsive and low-frequency structural resonance systems have shown to effectively remove ice, but mechanical stresses imparted to the blades have also show to damage composite structures and decrease fatigue life of the blade d-spar. A nonthermal system to protect from ice accretion to helicopter rotor blades has not been developed to the date.

At the Pennsylvania State University, the authors [10] continue research on a new approach to use piezoelectric actuators to cause instantaneous ice delamination. The ultrasonic energy is focused at the ice interface and takes advantage of the low shear adhesion strength of ice. Ultrasonic piezoelectric actuators have demonstrated the capability of delaminating thin ice layers of freezer ice (less than 3 mm) without any time delay after the actuator is turned on. The nonthermal system can also prevent ice formation at high ultrasonic stress regions.

Prior work by Palacios et al. [10], demonstrated that freezer ice can be instantaneously delaminated by the effects of ultrasonic excitation. To achieve ice debonding, it is important to ensure impedance matching between the actuator and the power source, and to also provide interface transverse shear stresses exceeding the adhesion strength of the accreted freezer ice. As ice accretes to the surface of the host structure transverse shear stresses are generated at the ice interface. Shear stresses created by centrifugal forces increase with ice thickness. The delamination process induced by transverse shear stresses is explained by Jones [11]. Ultrasonic excitation introduces additional ice-interface transverse shear stresses that promote ice debonding, which occurs as the transverse shear stresses exceed the shear adhesion strength of ice.

Freezer ice formation physics differs from the formation of in-flight icing. For this reason, de-icing systems must be tested under impact-icing conditions representative of in-flight icing. As described in [12], the adhesive shear strength of rime and glaze ice (the two types typically encountered in helicopter rotors) ranges between 0.12 and 1.0 MPa. The shear strength of rime ice is lower than that of glaze ice because it shears cohesively rather than at the ice–substrate interface [13]. In this paper, results obtained from wind-tunnel icing testing of ultrasonic de-icing systems are presented and correlated to finite element predictions.

II. Objectives

Because of the different shear adhesion strength and density of freezer ice versus wind-tunnel ice, experimental testing of ultrasonic excitation under wind-tunnel testing is sought to demonstrate the potential de-icing application of ultrasonic transverse shear excitation. The scope of this effort is to present proof-of-concept experimental results demonstrating instantaneous delamination of wind-tunnel ice to flat plates and airfoil-shaped structures under the effects of ultrasonic excitation. Experimental results were correlated with modeled predictions of transverse shear stresses at the ice interface responsible for ice delamination. To validate modeling tools, finite element predictions of the transverse shear stresses between the isotropic host structures (plates and airfoils) and an accreted ice layer under the effects of ultrasonic vibration were compared with experimental results. All the proof-of-concept experiments presented in this paper were conducted at Goodrich Icing Tunnel.

In this paper, two main sections describing the wind-tunnel icing experiments conducted on flat isotropic plates and NACA 0012 airfoils are presented.

III. Flat-Plate Testing and Finite Element Model Correlation

A. Wind-Tunnel Ice Experiments on Isotropic Plates

A $30.48 \times 30.48 \times 0.1$ cm ($12 \times 12 \times 0.04$ in.) steel plate was tested under the effects of wind-tunnel icing in the Goodrich Icing Tunnel. The steel plate had three 76.2-mm-diam ultrasonic disk actuators bonded to it. The plate was mounted on two 2.54-cm-diam solid aluminum bars that connected the 55.8-cm-wide (22-in.-wide) cross section of the tunnel test section. A schematic of the test specimen mounted on the clamping bars of the test section is illustrated in Fig. 1. To avoid flutter, two brass reinforcement bars (4 mm thick) were bolted at the edges of the steel plate.

Three actuators were mounted to the plate surface protected from impact water particles. The actuators were driven at 32 kHz, a frequency corresponding to a radial mode of the actuators bonded to the steel plate. The impedance of the driving electronics was set to 100 Ω, which is impedance value of the system at the ultrasonic

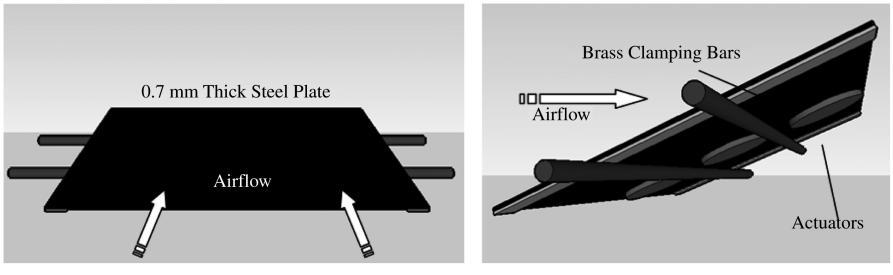

Fig. 1 Schematic of 30.48 × 30.48 mm 0.71-mm-thick steel plate mounted to the test section.

Table 1 Triple-actuated steel-plate test matrix

Test	Angle of attack, deg	Airspeed, m/s	LWC, g/m^3	Air temp, °C	MVD, μm	Spray time, actuator off, s	Power, W
1	−3	67	1	−4.5	40	0	100
2	−30.	67	0.5	−4.5	20	0	100
3	−30	67	0.5	−4.5	20	0	150

frequency of 32 kHz. The selected driving mode (32 kHz, 100 Ω) was identified experimentally using an impedance analyzer. The electrical impedance of the actuators load was matched with the impedance of the amplifier to maximize input power, as described in [14].

The tests conducted on this specimen are summarized Table 1. During all tests, ice was prevented from forming around the actuator locations at a maximum input power density of 0.7 W/in.^{2}. Ice shedding was observed on the leading edge, trailing edge, and on top of the reinforcing brass bars once ice accumulation reached a critical thickness of approximately 1.2 mm in thickness, as shown in Fig. 2. In this same figure, the ice accretion to the plate with the actuators turned off is shown.

B. Wind-Tunnel Ice Experiment on a D-Spar Representative Composite Plate

A test was performed on a composite plate representative of a D-spar area of a helicopter rotor blade. This coupon was provided by Bell Helicopters, a Textron Company. The proof-of-concept test was performed to demonstrate that actuation of composite structures, representative of a leading-edge helicopter blades, is possible. A 76.2-mm-diam, 2.54-mm-thick lead zirconate titanate (PZT)-4 disk was bonded directly to the stainless steel erosion-protection cap. The plate was placed in the icing wind tunnel at a 3 deg nose-down angle of attack. During the test the actuator remained turned on during spraying with a net input power of 60 W. At wind speeds of 150 mph (67 m/s), liquid water content (LWC) of 1 g/m^3, water particle medium volume diameters of 40 μm and a temperature of −4.5°C, the actuator continuously shed off accreted ice on the leading edge of the plate, maintaining the area clean of ice exceeding a critical thickness. Ice shedding was observed only on those areas where concentrated stresses were created (discontinuities of the stainless steel erosion cap). Thin layers of ice accreted to the surface of the protection cap could not be removed. A second run at the same wind-tunnel conditions was performed. During this second run, the actuator remained turned off. Leading-edge ice accretion is observed after 5 min of spraying as shown in Fig. 3.

C. Ultrasonic Actuators: Isotropic Flat-Plate Finite Element Modeling

Piezoelectric effects occur in noncentrosymmetric crystals, such as PZT and quartz. Electric dipoles are generated due to mechanical deformations. The converse effect (reverse piezoelectric effect) has been used in this research to generate transverse shear stresses between a host structure and ice in order to debond the freezer ice.

The following summarized finite element method derivation is described in detail in [15–19]. The constitutive equations for piezoelectric materials under small field conditions are defined in Equation (1):

$$T_{ij} = c^E_{ijkl} S_{kl} - e_{kij} E_K \qquad D_i = e_{kij} S_{kl} + \varepsilon^S_{ij} E_j \tag{1}$$

where D is the electric displacement vector (C/m^2), S is the strain vector, E is the applied external electric field vector (V/m), and T is

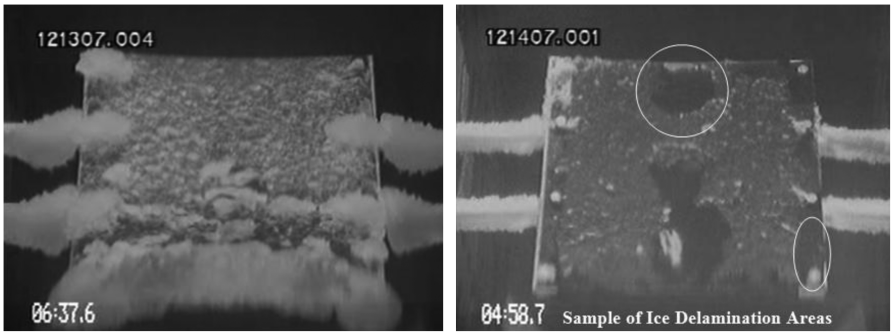

Fig. 2 Photographs of 30.48 cm × 30.48 cm × 0.7 mm thick steel plate: a) ice accretion with actuators off and b) after test 1 with a triple ultrasonic disk actuator system.

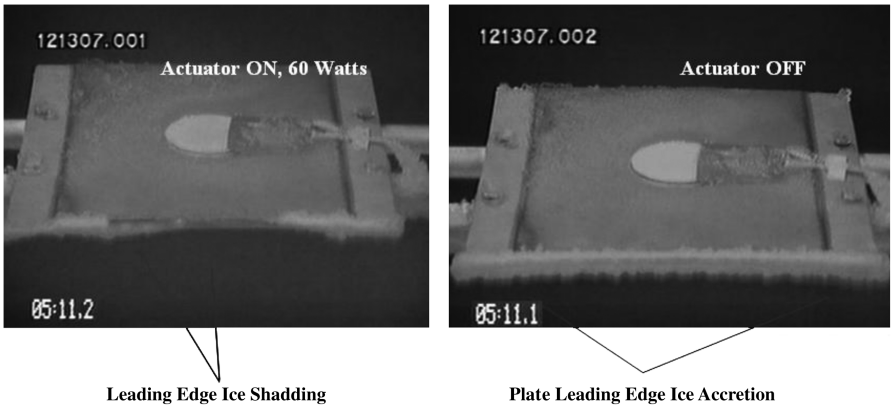

Fig. 3 Composite coupon impact-icing test, actuator on vs actuator off results (5 min spraying time, 150 mph, 1 g/m^3,40 μm).

the stress vector (N/m^2). The elastic stiffness at constant electric field, c^E, the piezoelectric coupling, e, and the dielectric stiffness at constant strain, ε^S, are assumed to be constant, which is a reasonable assumption for piezoelectric materials subjected to moderate electric fields (and therefore small deformations).

From the stationary condition, and looking into the harmonic behavior of the system (reverse piezoelectric effect at various input frequencies), the following relation arises as Q (electrical excitation applied to the PZT material) is nonzero:

$$\begin{bmatrix} K_{uu} & K_{u\varphi} \\ K_{u\varphi}^T & K_{\varphi\varphi} \end{bmatrix} \begin{bmatrix} U \\ \varphi \end{bmatrix} = \begin{bmatrix} F \\ -Q \end{bmatrix} \tag{2}$$

Note that no forces are applied to the actuator; therefore, F is zero. Harmonic analysis is performed to calculate the impedance of the system at different frequencies. This analysis describes the response of the piezoelectric actuator/steel-plate/ice system due to an applied external electric potential to the PZT actuator at an angular frequency ω (φ applied to the electrodes). The electrical current entering the electrodes is written as $I = j\,\omega\,Q$. Therefore, the impedance Z of each electrode is given by the ratio φ/I. The frequency dependent impedance values are used to determine the actuator-structure resonance frequency. Resonating ultrasonic modes occur at those frequencies where the ultrasonic actuator provides a maximum current output for a given driving voltage. The displacement and stress fields in the structure are calculated at any selected driving frequency.

After the experiments were conducted, finite element analysis of the PZT actuators bonded to the isotropic plate (and covered by a 1.2-mm-thick ice layer) was conducted to predict the impedance response of the system. The predicted results are show in Fig. 4. The impedance value of the selected ultrasonic mode agreed with the experimentally measured mode with a discrepancy of less than 5% on both frequency and impedance value.

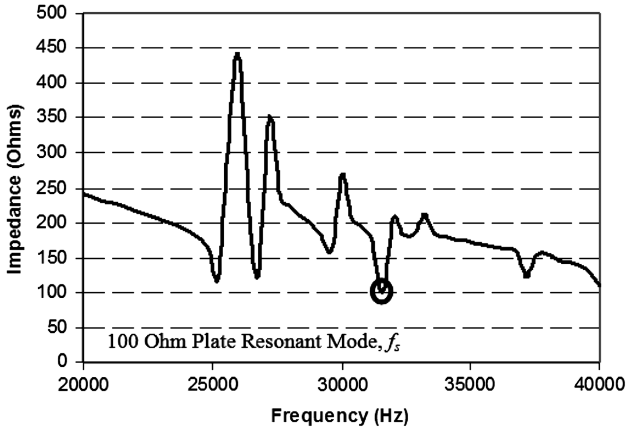

Fig. 4 Triple-disk actuator predicted impedance and driving mode.

The impedance of the system is defined as the ratio of the voltage, V, to the current, I, in the alternating-current circuit. A low peak of the impedance implies that the input voltage becomes a minimum at the same time as the current becomes a maximum. The frequency corresponding to an impedance low is that of a resonance mode, f_s. During testing, the radial mode of the actuator was triggered. This mode is predicted to occur at a frequency of 32 kHz. In the impedance graph shown in Fig. 4, there can be seen other ultrasonic modes indicated by impedance lows. These modes have higher impedance than the pure radial mode of the actuator and are triggered by other resonances of the systems. These modes were also tested during benchtop testing to provide lower de-icing capabilities than the pure radial mode of the actuator.

The ice-layer thickness used during the modeling was determined by the critical ice thickness shed during wind-tunnel icing tests, which were presented in the prior section. The test-section clamping bars that hold the plate in place inside the wind tunnel were modeled by clamping the surfaces of the plate edge, as shown in Fig. 5.

The transverse shear stresses responsible for ice delamination and generated by the PZT disks (100 W input) at the ice interface were calculated for the 32 kHz ultrasonic radial mode with 100 Ω impedance. Modeled predictions were compared with the ice-shedding patterns observed during wind-tunnel testing, and they are presented in Fig. 6. The frequency of the predicted ultrasonic mode agreed with the experimentally observed driven mode actuated during tests 1 to 3 with an error of 1.25%. The areas with concentrated transverse shear stress that were predicted by means of finite element models also agreed with the shedding areas observed during the impact-icing experiments. The shear adhesion strength of the impinging ice was not directly measured during tests, but finite element modeling of the system predicted up to 5 MPa at the interface of a 1.2-mm-thick ice layer on areas where experimental debonding was observed (100 W input power to the actuators). The power density was experimentally measured to be 1.2 W/cm^2.

IV. Airfoil-Shaped Icing Tests and Model Correlation

A. NACA0012 with Two Ultrasonic Actuators

Ice accretion patterns collected on flat plates are not representative of ice shapes encountered on helicopter blades. Wind-tunnel ice accretion tests were conducted on a NACA 0012 airfoil. The span of the airfoils was 56 cm. The chord of the airfoil was 35.5 cm. The leading edge of the airfoils (30% chord from leading edge), were made out of 1-mm-thick aluminum. Two 8-mm-thick aluminum ribs made and a 8 mm spar provided a structural surface to bolt the leading-edge and trailing-edge airfoil skin (also 1-mm-thick aluminum). A photograph of the airfoil as placed in the tunnel test section is presented in Fig. 7.

Two PZT-4 ultrasonic disks (76.2 mm diameter, 2.54 mm thick) where placed 4 cm from the edge of one external rib of the airfoil and

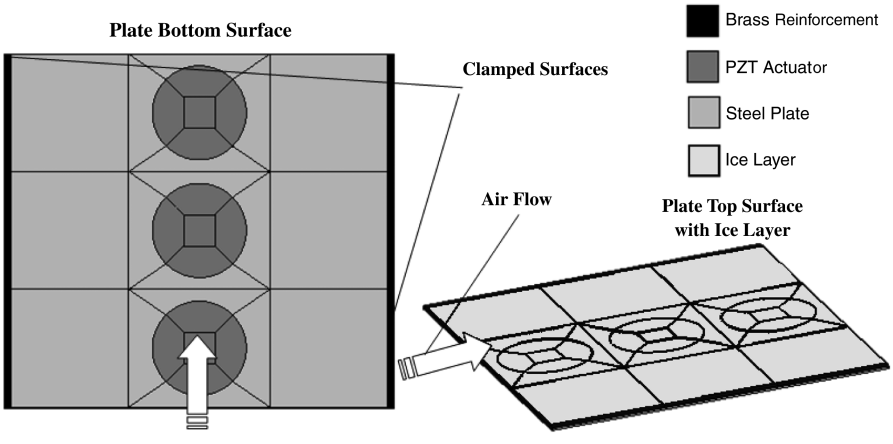

Fig. 5 Steel plate, PZT disk, ice-layer finite element model.

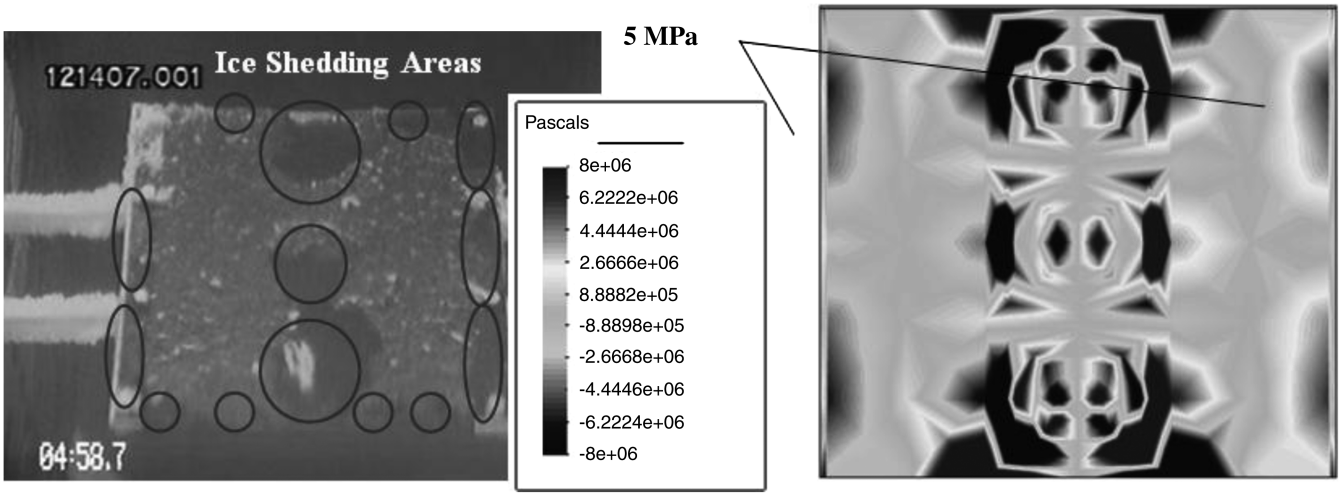

Fig. 6 Comparison between experimental impact-ice-shedding and ice-interface predicted transverse shear stresses responsible for ice delamination (100 W).

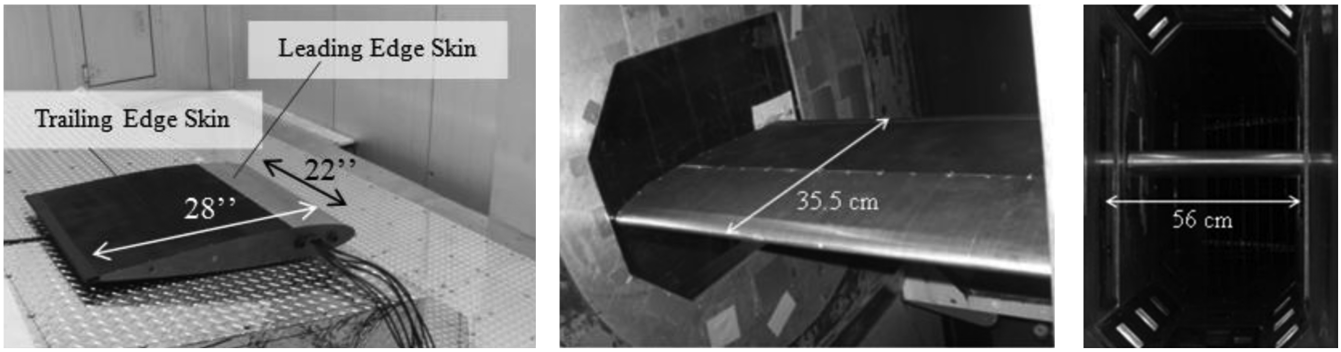

Fig. 7 NACA 0012 photographs and model mounted in the test section of the Goodrich Icing Tunnel.

4 cm from the end of the aluminum leading-edge cap. Detail of the actuators bonded to the aluminum leading-edge cap is shown in Fig. 8.

Baseline ice accretion shapes (actuator off) were obtained for an icing cloud formed by20-μm-diam water droplets and a liquid water concentration of 1.5 g/m^3. The temperature in the test section was -15°C and the flow velocity was 67 m/s. The NACA 0012 airfoil was placed in the test section with a nose-down angle of attack of 3°. The spray time was 3 min. The baseline ice accretion shape is depicted in Fig. 9. In this same figure, the ice removal capabilities of the ultrasonic excitation is also shown.

The two PZT-4 actuators were driven at their radial ultrasonic mode (32 kHz) and at an impedance value of 100 Ω. 300 W were applied to the actuators (170 V). The same icing conditions created during the baseline test were repeated. The actuators remained turned on during the 3 min of spraying time. Constant ice shedding was observed in the leading-edge region directly in front of the actuators. Thin layers of ice (less than 1 mm thick) constantly delaminated from the leading edge of the airfoil in this specific area. Five centimeters away from the edge of the actuator in the span direction and toward the other end of the airfoil, ice continued to accrete until it reached a thickness of approximately 0.5 cm. When the ice thickness reached 0.5 cm (2 min of spraying time), the ice shape spanning from 5 cm away from the actuator edge in the span direction to the edge of the airfoil (40 cm) shed off completely from the leading edge. Thin layers of ice continued to be shed off from the entire leading-edge area until the icing nozzles were shut off. A photograph of the post test ice accretion observed in the leading edge of the airfoil is shown in Fig. 9. Detail of the two identified regions (constant ice-shedding area and ice accretion up to 0.5 cm area) is depicted in Fig. 10.

It was observed how the ultrasonic excitation provided by the two PZT-4 disks prevented considerable ice formation on the airfoils leading-edge area up to 5 cm away from the actuator in the span direction (constant ice-shedding area). The excitation also removed ice shapes further away from the actuator excitation when the thickness of the accreted ice reached values of up to 0.5 cm. Finite

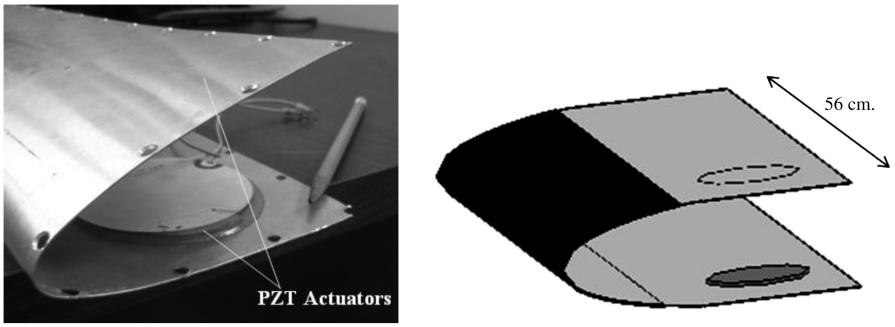

Fig. 8 Schematic and photograph of ultrasonic actuators bonded to the leading-edge cap of a NACA 0012 airfoil.

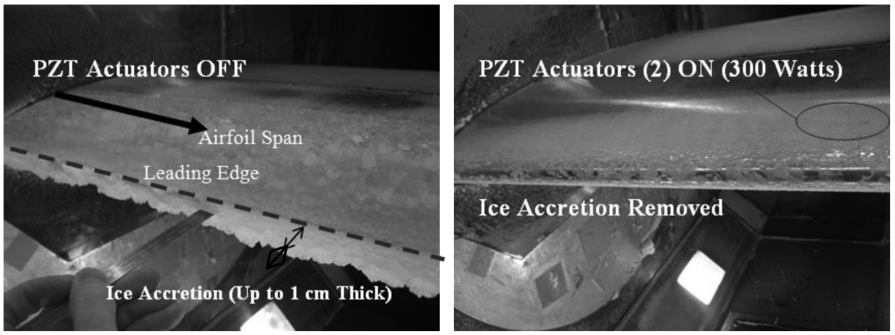

Fig. 9 Ice accretion shapes obtained without and with ultrasonic actuation (20 μm, 1.5 g/m^3, −15°C, 67 m/s, −3° angle of attack, 3 min spray time).

element modeling of the leading edge with accreted ice was performed and compared with experimental results. Transverse shear stress concentration patterns agree with ice delamination patterns. Constant ice delamination of thin layers of ice is observed in areas up to 5 cm away in the span direction from the actuator location, where transverse shear stresses are concentrated. In areas farther away, the stress concentration diminishes for a 1-mm-thick ice layer. Higher ice thickness is required to promote ice-interface stresses large enough to promote ice shedding. Experimental ice-shedding patterns are consistent with model predictions, as high ice-interface shear stresses are identified on leading-edge areas right in front of the actuator on the chordwise direction, while reduced stresses are seen on the remaining areas of the leading edge for a 1-mm-thick ice layer. Higher ice thickness is required to promote ice delamination. Modeling results are depicted in Fig. 10, in which the transverse shear stresses at the ice interface are shown.

B. NACA0012 with Eight Ultrasonic Actuators

In a second set of experiments, and to demonstrate the capability of ultrasonic actuators to provide instantaneous delamination of thin layers of ice on the complete leading edge, the number of ultrasonic actuators was increased from 2 to 8 on the NACA 0012 model. A schematic and predicted ice-interface transverse shear stresses are shown in Fig. 11. To reach comparable ice-interface stresses as those predicted for two actuators, the input power was reduced to 200 W, 65% of the power required during the first NACA0012 test conducted. The power density was measured to be 1 W/cm^2, close to 72% power density reduction with respect to electrothermal systems (3.8 W/cm^2). The transverse shear stresses are distributed at the interface of the 1 mm ice layer modeled. As ice accreted to the airfoil, continuous ice delamination of thin layers of ice is expected.

Tests were conducted at the same icing conditions as the test in which only two actuators were present (mean volumetric diameter

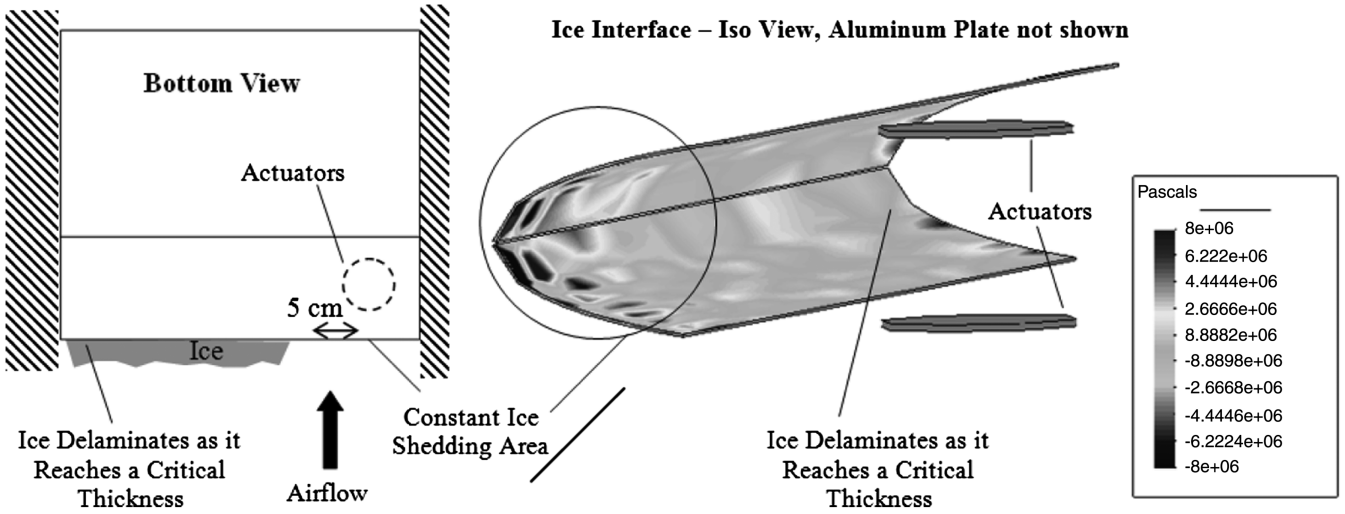

Fig. 10 Schematic of ice accretion regions identified during testing of NACA 0012 airfoil and modeling results at 32 kHz, 300 W. Ice-layer thickness is 1 mm (0.9 g/m^3, 9.1 GPa).

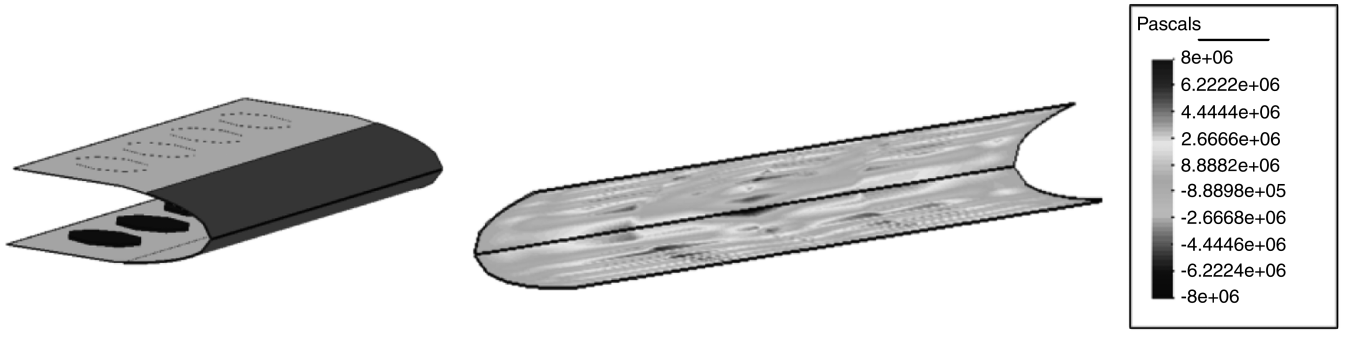

Fig. 11 Schematic of aluminum leading edge of model with eight PZT ultrasonic disks. Note distributed transverse shear stress at the ice interface cover entire leading edge area (200 W Input).

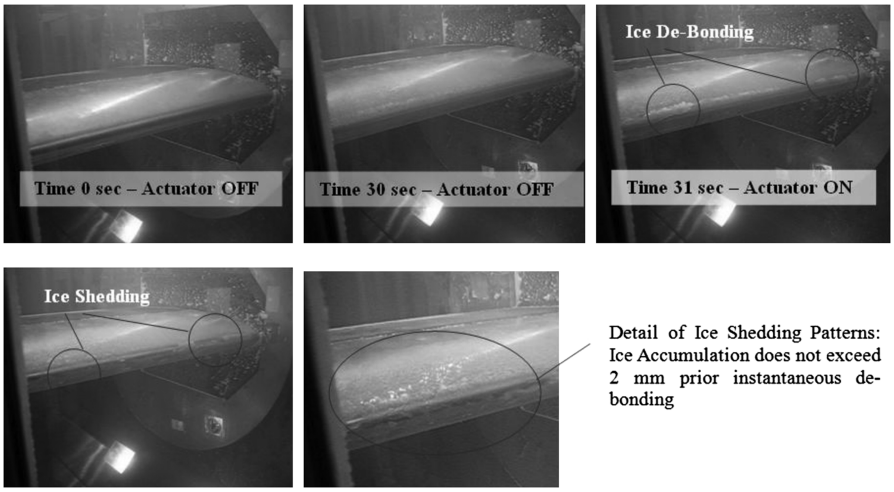

Fig. 12 Photographs taken during testing of eight actuators; instantaneous and continuous ice delamination (∼1-mm-thick ice layers) observed on airfoil leading edge (200 W).

[MVD] was 20 μm, LWC was 1.5 g/m^3, temperature was −15°C, velocity was 67 m/s, and angle of attack was 3 deg). As predicted, constant ice delamination of thin layers of ice (approximately 1 mm thick) was observed on the airfoil. The experimental results observed during testing are summarized on Fig. 12.

The measured weight of the electronics used to power the ultrasonic model was 19.5 kg (43 lb). Initial estimates indicate that this weight could be reduced as much as 25% if power amplifiers, designed to trigger a specific ultrasonic mode, would be used.

The majority of the weight introduced by electrothermal de-icing is due to power systems. Ultrasonic de-icing techniques present the potential to reduce the weight of such power systems by close to 85%. The weight of distributed PZT actuators embedded in the leading edge of a representative rotor blade (14.6 m diameter assumed) is estimated to be 7.7 kg (17 lb). The weight of the ultrasonic actuators is conceptualized to be a replacement of leading-edge masses (typically lead) currently used to introduce rotor inertia and to move the center of gravity of the blade forward of the aerodynamic center.

V. Conclusions

Wind-tunnel testing of flat plates and NACA 0012 isotropic airfoils under the effects of ultrasonic excitation was conducted. The nonthermal ultrasonic vibration promoted ice-interface transverse shear stresses that instantaneously delaminated layers of accreted ice (measured to be as thin as 1 mm). This novel nonthermal, low-power de-icing approach decreases the required power by over 70% with respect to currently used electrothermal de-icing. The concept also avoids drawbacks related to electrothermal de-icing, such as potential localized melting of composite structures or lack of heat propagation on nonmetallic leading edges.

Based on the results obtained during this experimental investigation, the following conclusions are made:

1) Piezoelectric actuators excited at their radial resonance (32 kHz) are able to debond wind-tunnel ice layers of approximately 1.2 mm thickness from areas where transverse shear stresses exceed the adhesion strength of ice to isotropic plates.

2) Proof-of-concept wind-tunnel icing tests conducted on flat plates demonstrated that ice debonding areas agreed with locations where finite element predictions presented concentrated transverse shear stresses. Predicted ultrasonic transverse shear stress values of up to 5 MPa were calculated on areas where experimental ice debonding was observed. Ice accretion was completely prevented on those areas where maximum transverse shear stresses were calculated: specifically, on top of the actuator region. In those areas where transverse shear stresses were large enough to debond ice layers, de-icing was accomplished with an estimated power consumption of 1.2 W/cm^2.

3) The predicted transverse shear stresses required to debond impact-ice layers exceeded the quantified shear adhesion strength of both rime and glaze ice by up to five times. For this reason, higher input power was required to instantaneously debond wind-tunnel accreted ice, as compared with predictions or freezer ice.

4) Proof-of-concept experiments conducted on a composite flat-plate coupon representative of a leading D-spar proved that instantaneous ice removal on structures with a stiffness representative of leading-edge helicopter blades is possible using ultrasonic excitation as long as stress concentration regions, such as material discontinuities are present.

5) Airfoil leading-edge ice debonding using ultrasonic excitation was demonstrated on a 35.5 cm chord NACA 0012 aluminum airfoil (1 mm thick) subjected to impact-icing conditions. Ice layers of approximately 1 mm in thickness were continuously debonded avoiding ice accretion on the airfoils leading edge. The input power densities were measured to be as low as 1 W/cm^2, or 72% less power density than electrothermal de-icing system requirements (3.8 W/cm^2). Initial weight estimates indicate that the power supply to ultrasonic de-icing concepts could up to 85% less than the weight of power systems used for electrothermal de-icing. This calculation assumes that the weight of PZT actuators embedded in the leading edge of the blade replaces leading-edge masses currently installed in this same location.

6) Ultrasonic transverse shear stresses increased as the accreted ice-layer thickness increased. Ice delamination is reached at locations with reduced transverse shear stresses as the ice thickness reaches a critical value. The critical thickness for ice shedding can be reduced by increasing actuator power density.

Ultrasonic de-icing has demonstrated its capabilities to continuously shed thin layers (less than 1 mm) of impact icing during wind-tunnel testing, preventing ice formation on the leading edge of airfoil structures. This low-power, nonthermal approach could provide rotor blade de-icing in the future as the technology advances and blade implementation challenges are addressed.

Acknowledgments

The authors would like to thank the U.S. Army and the Aviation Applied Technology Directorate (AATD) for sponsoring this research. Initial work presented on this research regarding impact-icing tests to flat plates is partially funded by the U.S. Army Rotorcraft Centers of Excellence under agreement no. W911W6-06-2-0008. Work done regarding airfoil-shaped structures is partially funded by Phase II Small Business Innovation Research provided by the Aviation Applied Technology Directorate to FBS Worldwide, Inc. (contract no. W911W6-08-C-0064). The authors would also like to thank Galdemir Botura for graciously allowing us to use the Goodrich Icing Wind Tunnel, as well as Bell Helicopters, a Textron

Company, for partially funding this research (icing wind-tunnel testing of plates excited by ultrasonic vibration). The views and conclusions contained in this document are those of the authors and should not be interpreted as representing the official policies, either expressed or implied, of the U.S. Government.

References

[1] Withington, T., "Bad Vibrations," *Aerosafety World*, Vol. 5, No. 1, Feb. 2010, pp. 26–28.

[2] Flemming, R., Alldridge, P., and Doeppner, R., "Artificial Icing Tests of the S-92 Helicopter in the Mckinley Climatic Laboratory," 42nd AIAA Aerospace Sciences Meeting and Exhibit, Reno, NV, AIAA Paper 2004-737, Jan. 2004.

[3] Flemming, R., and Lednicer, D., "Correlation of Airfoil Icing Relationships with Two-Dimensional Model and Full Scale Rotorcraft Icing Test Data," 23rd AIAA Aerospace Sciences Meeting, Reno, NV, AIAA Paper 1985-337, Jan. 1985.

[4] Flemming, R., Murty, H., Papadakis, M., and Wong, S., "The Design, Fabrication, and Testing of Simulated Ice Shapes for the S-92A Helicopter," 42nd AIAA Aerospace Sciences Meeting and Exhibit, Reno, NV, AIAA Paper 2004-736, Jan. 2004.

[5] Coffman, H. J., "Helicopter Rotor Icing Protection Methods," *Journal of the American Helicopter Society*, Vol. 32, No. 2, April 1987, pp. 34–39.
doi:10.4050/JAHS.32.34.

[6] Reinmann, J. J., Shaw, R. J., and Ranaudo, R. J., "NASA's Program on Icing Research and Technology," *Proceedings of the Symposium on Flight in Adverse Environmental Conditions*, Kluwer, Norwell, MA, May 1989, pp. 73–78.

[7] Martin, C. A., and Putt, J. C., "Advanced Pneumatic Impulse Ice Protection System (PIIP) for Aircraft," *Journal of Aircraft*, Vol. 29, No. 4, 1992, pp. 714–716.
doi:10.2514/3.46227

[8] Venna, S. V., Lin, Y., and Botura, G., "Piezoelectric Transducer Actuated Leading Edge De-Icing with Simultaneous Shear and Impulse Forces," *Journal of Aircraft*, Vol. 44, No. 2, March–April 2007, pp. 510–515.

[9] Palacios, J. L., and Smith, E. C., "Dynamic Analysis and Experimental Testing of Thin-Walled Structures Driven By Shear Tube Actuators," *46th AIAA/ASME/ASCE/AHS/ASC Structures, Structural Dynamics & Materials*, AIAA, Reston, VA, 2005, pp. 3862–3875; also AIAA Paper 2005-2112.

[10] Palacios, J., Smith, E., Rose, J., and Gao, H., "Ultrasonic Shear Wave Anti-Icing System for Helicopter Rotor Blades," *62nd Annual Forum Proceedings–American Helicopter Society*, AHS International, Alexandria, VA, May 2006, pp. 1492–1502.

[11] Jones, R., *Mechanics of Composite Materials*, Taylor and Francis, Philadelphia, 1999.

[12] Chu, M. C., and Scavuzzo, R. J., "Adhesive Shear Strength of Impact Ice," *AIAA Journal*, Vol. 29, No. 11, Nov. 1991, pp. 1921–1926.
doi:10.2514/3.10819

[13] Scavuzzo, R. J., Chu, M. L, and Kellackey, C. J., "Impact Ice Stress in Rotating Airfoils," *Journal of Aircraft*, Vol. 28, No. 7, July 1991, pp. 450–455.
doi:10.2514/3.46048

[14] Someda, C., *Electromagnetic Waves*, Chapman and Hall, London, 1998, pp. 284–295.

[15] Sirohi, J., and Chopra, I., "Fundamental Understanding of Piezoelectric Strain Actuators," *Journal of Intelligent Material Systems and Structures*, Vol. 11, No. 4, 2000, pp. 246–257.

[16] Jarng, S., "Comparison of Barrel-Stave Sonar Transducer Simulation Between a Coupled FE-BEM and ATILA," *IEEE Sensors Journal*, Vol. 3, No. 4, 2003, pp. 439–446.
doi:10.1109/JSEN.2003.815846

[17] Uchino, K., *FEM and Micromechatronics with ATILA Software*, Taylor & Francis, Philadelphia, May 2008.

[18] *ATILA Finite Element Code for Piezoelectric and Magnetostrictive Transducer Modeling Version 5.03 User's Manual*, Institut Supérieur d'Electronique du Nord, Lille, France, July 2005, pp. 35–38.

[19] Safari, A., and Akdogan, E. K. (eds.), *Piezoelectric and Acoustic Materials for Transducer Applications*, Springer, New York, 2008, pp. 241–257, Chap. 12.